Homework 11 Stress Report

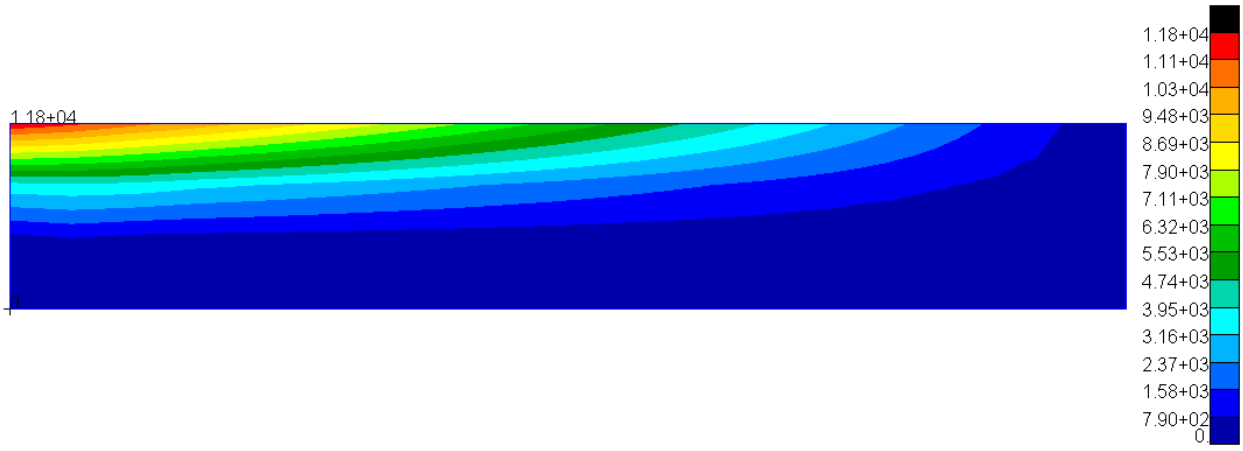

Tiger Sievers

Instructor: Dr.Richard Hale

THE UNIVERSITY OF KANSAS

Department of Aerospace Engineering

May 30, 2025

Executive Summary

This report evaluates the stress and displacement behavior of a beam structure using both triangular and rectangular membrane elements in finite element models, compared against a classical beam theory reference model. The primary objective was to assess the convergence characteristics of stress and displacement outputs with increasing mesh refinement and to validate the numerical models against analytical expectations.

Results Overview

- The theoretical maximum normal stress from beam theory was calculated to be **12,000 psi**, occurring at the extreme fiber under bending.
- Simulation results from PATRAN confirmed this value; however, boundary condition artifacts prompted the use of the second element from the end as a consistent comparison point.
- Maximum displacement from numerical models closely matched the analytical beam theory solution.

Stress Convergence

Stress convergence was assessed based on the maximum principal stress values across successive mesh refinements.

Meshing Type	% Error in Max Principal Stress
Rectangular	1.80%
Triangular	9.72%

Table 0.0.1 Stress Convergence between Final Iterations

Displacement Convergence

Displacement convergence was tracked at the free end of the beam, with models demonstrating close agreement with beam theory predictions.

Model	DOFs	Max Displacement (in)
Rect3	2808	-8.798×10^{-2}
Tri3	2808	-8.652×10^{-2}
Beam	6	-8.829×10^{-2}

Table 0.0.2 Displacement Comparison with Beam Theory

While both meshing strategies approach convergence with increasing refinement, the rectangular meshing scheme exhibits superior convergence characteristics in both stress and displacement results. At lower mesh densities, triangular elements introduce higher numerical error but converge toward beam theory values with finer meshing. These findings highlight the importance of mesh quality and refinement in finite element simulations, particularly near high-stress or constrained regions.

Contents

List of Figures

List of Tables

1. Introduction

This report presents a finite element analysis of a cantilevered beam structure subjected to a uniformly distributed load, following the convergence study guidelines provided. The primary objective is to evaluate the convergence behavior of both stress and displacement as the mesh is refined, using two distinct finite element modeling strategies: triangular membrane elements and rectangular membrane elements.

The beam has dimensions of 18.0 in $\times$ 3.0 in with a thickness of $t = 0.1$ in, and is modeled with material properties of $E = 10^7$ psi, $G = 3.8 \times 10^6$ psi, and Poisson's ratio $\nu = 0.32$. A uniformly distributed load of $P = 100$ lb is applied along the top edge of the beam. Fixed boundary conditions are applied to the left edge, simulating a cantilevered constraint.

Three mesh refinements are created for each meshing strategy to study convergence. The results focus on two key quantities of interest: the maximum principal stress along the top surface of the beam and the maximum vertical displacement at the free end. These results are then compared to classical beam theory predictions to assess the fidelity of each modeling approach.

2. Geometry

Each model in this analysis is based on a rectangular geometry with dimensions of 18 in × 3 in and a thickness of 0.1 in. This consistent baseline geometry was discretized using two meshing strategies: quadrilateral (quad) and triangular (tria) membrane elements. To evaluate convergence behavior, each meshing type was refined across three levels of increasing density.

Table 2.0.1 summarizes the meshing details for each model, including the number of elements, nodes, and associated degrees of freedom (DOFs). The DOF count directly reflects the resolution and complexity of each finite element model, increasing significantly with mesh refinement.

Table 2.0.1 Model Meshing for Model

Model	Meshing Type	# Elm	# Nodes	DOFs
Rect1	Quad	54	58	126
Rect2	Quad	216	259	756
Rect3	Quad	864	877	2808
Tri1	Tria	108	76	126
Tri2	Tria	108	231	672
Tri3	Tria	432	949	2808

Figures 2.0.0.1 and 2.0.0.2 display the lowest and highest quadrilateral mesh densities, respectively. As evident in Table 2.0.1 , refinement increases both the element count and the total number of nodes, resulting in higher model resolution and computational demand.

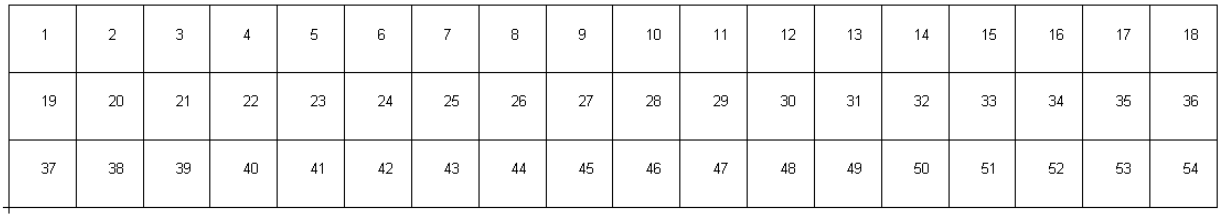

Fig. 2.0.0.1 Rect1 Mesh Geometry

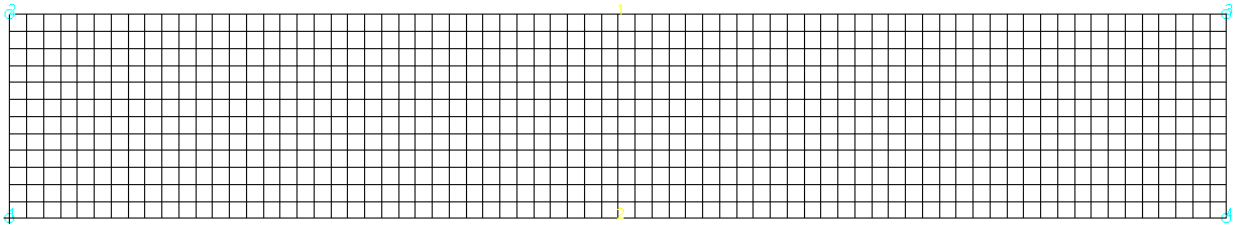

Fig. 2.0.0.2 Rect3 Mesh Geometry

Figure 2.0.0.3 illustrates a representative triangular mesh model. While triangular elements offer greater flexibility in meshing complex geometries, they often require a higher element count to achieve the same level of accuracy or degrees of freedom as quadrilateral elements.

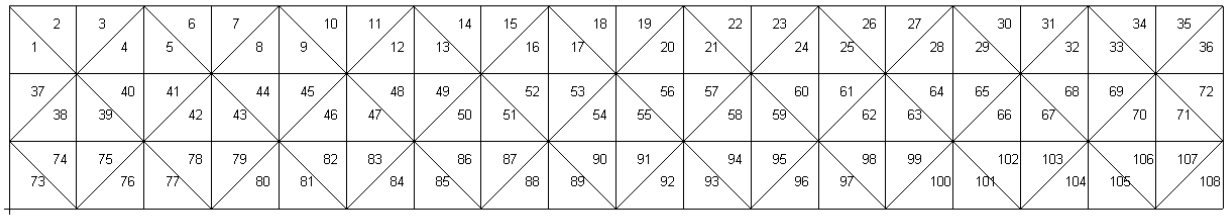

Fig. 2.0.0.3 Example of Triangular Mesh

3. Loading and Boundary Conditions

3.1 Support Conditions

The left edge of the beam is constrained with a fully fixed (clamped) boundary condition. This boundary condition restricts all translational and rotational degrees of freedom. The applied constraints prevent any displacement in the x, y, or z directions, as well as any rotation about those axes. This ensures that all deformation resulting from the applied load occurs within the beam body, allowing accurate tracking of displacement and stress propagation.

Table 3.1.1 Boundary Condition Summary

Edge	u_x	u_y	u_z	θ_x	θ_y	θ_z
Left Edge	0	0	0	0	0	0

3.2 Applied Loads

A uniformly distributed load is applied along the right edge of the beam, opposite the fixed end. This load is applied in the negative y-direction to simulate downward loading and produces bending across the length of the cantilevered beam. The total load magnitude is 100 lb, distributed evenly across the edge to simulate surface pressure converted to equivalent nodal forces within the PATRAN/NASTRAN [1] model.

Table 3.2.1 Nodal Load Definition

Edge(s)	$\mathbf{F_y}$ [lb]
Right Edge	-100.0

4. Material Properties

The beam is modeled using a single, homogeneous, isotropic material assumed to behave in a linear-elastic manner throughout the analysis. No failure criteria, plastic deformation, or material nonlinearity are considered. This assumption is appropriate for the purpose of evaluating elastic stress and displacement convergence under small-strain conditions.

The mechanical properties used in the finite element models are summarized in Table 4.0.1 .

Table 4.0.1 Assumed Mechanical Properties of the Structural Material

Property	**Value**
Young's Modulus, E	10×10^6 psi
Shear Modulus, G	3.8×10^6 psi
Poisson's Ratio, ν	0.32

5. Finite Element Model

The cantilevered beam was modeled using seven distinct finite element configurations, varying by both mesh density and element type. Two meshing strategies were employed: quadrilateral (quad) membrane elements and triangular (tria) membrane elements. These configurations allow for a comparative analysis of convergence behavior based on element topology and mesh refinement.

The quadrilateral meshes were constructed with increasing resolution, starting from 54 elements in the coarsest model (Rect1) up to 216 elements in the most refined model (Rect3). Similarly, triangular models were constructed from 108 elements in Tri1 to a highly refined mesh with 1728 elements in Tri3. The corresponding degrees of freedom (DOFs) increase with mesh refinement, as shown in Tables 5.0.1 and 5.0.2 .

Model	# of Elements	Degrees of Freedom
Rect1	54	216
Rect2	108	756
Rect3	216	2808

Table 5.0.1 Quadrilateral (Quad) Meshed Models

Model	# of Elements	Degrees of Freedom
Tri1	108	216
Tri2	384	672
Tri3	1728	2808

Table 5.0.2 Triangular (Tria) Meshed Models

All models apply the same boundary and loading conditions to ensure consistent comparison. The beam is fully fixed along the left edge, constraining all translational and rotational degrees of freedom, effectively simulating a classical cantilever. A total downward force is applied along the right edge using a Total Load approach in PATRAN/NASTRAN [1], distributing the force proportionally across nodes. This method ensures that the total load remains constant regardless of mesh density, enabling fair comparison across models.

6. Analysis & Results

6.1 Maximum Normal Stress in a Beam

The maximum normal stress in a beam under bending occurs at the extreme fibers (top or bottom) of the beam's cross-section. This stress is calculated using the formula:

$$\sigma = \frac{My}{I}$$

where M is the bending moment, y is the distance from the neutral axis to the point of interest, and I is the second moment of area of the beam's cross-section. The maximum normal stress, $\sigma_{\max}$, occurs at the surface of the beam, where $y = y_{\max}$, the maximum distance from the neutral axis. Therefore, the maximum normal stress is given by:

$$\sigma_{\max} = \frac{My_{\max}}{I}$$

Calculating the maximum stress using the equation above, we get $12,000$ psi (in tension) at the top of the beam. This should be the maximum stress that the models converge to.

6.2 Maximum Principal Stress in Membrane Elements

The maximum principal stress in a membrane element represents the largest normal stress that acts on the element. This stress is determined by considering the state of stress at a point within the membrane element and finding the normal stress components that are oriented along the directions of maximum and minimum stresses.

Stress in Membrane Element In a membrane element, the stress components typically include normal stresses (σ_x) and (σ_y) and shear stress (τ_{xy}) in the plane of the element. These stresses are represented as:

$$\sigma_x = \text{Normal stress in the x-direction}$$

$$\sigma_y = \text{Normal stress in the y-direction}$$

$$\tau_{xy} = \text{Shear stress in the xy-plane}$$

These stresses are easily found in the F06 file produced by PATRAN [1], as shown in Figure 6.2.0.1 .

Calculating the Maximum Principal Stress The maximum principal stress, denoted as $\sigma_{\max}$, can be calculated using the following formula derived from the stress tensor for a 2D plane stress condition:

$$\sigma_{\max} = \frac{1}{2}\left(\sigma_x + \sigma_y\right) + \sqrt{\left(\frac{\sigma_x - \sigma_y}{2}\right)^2 + \tau_{xy}^2}$$

This formula provides the maximum normal stress in the material by considering both the normal and shear stresses acting at a point. The result $\sigma_{\max}$ is the largest stress, and it is oriented along the principal direction, which is perpendicular to the plane of maximum shear. This transformation is done by PATRAN [1] and shown in the F06 file.

S T R E S S E S I N Q U A D R I L A T E R A L E L E M E N T S (Q U A D 4) OPTION = BILIN

ELEMENT ID	GRID-ID	FIBER DISTANCE	STRESSES IN ELEMENT COORD SYSTEM NORMAL-X	NORMAL-Y	SHEAR-XY	PRINCIPAL STRESSES (ZERO SHEAR) ANGLE	MAJOR	MINOR	VON MISES
1	CEN/4	-5.000000E-02	7.792616E+03	1.048207E+03	4.393670E+02	3.7116	7.821118E+03	1.019704E+03	7.364405E+03
		5.000000E-02	7.792616E+03	1.048207E+03	4.393670E+02	3.7116	7.821118E+03	1.019704E+03	7.364405E+03
	1	-5.000000E-02	1.182403E+04	2.493637E+03	4.393670E+02	2.6901	1.184468E+04	2.472993E+03	1.082221E+04
		5.000000E-02	1.182403E+04	2.493637E+03	4.393670E+02	2.6901	1.184468E+04	2.472993E+03	1.082221E+04

Fig. 6.2.0.1 Sample F06 of QUAD Element

6.2.1 Maximum Principle Stress from PATRAN Model

For each meshing iteration, the maximum principal stress was output for the elements in the top row of the model. The maximum principle stresses for models Rect1, Rect2, and Rect3 are shown in Figures 6.2.1.1 ,6.2.1.3 ,and 6.2.1.5 respectively.

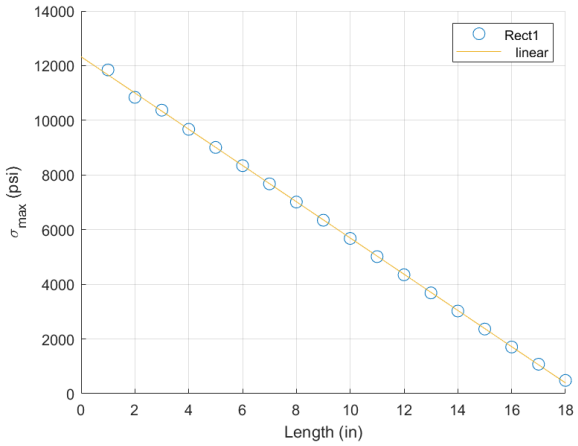

Fig. 6.2.1.1 Model Rect1 Maximum Principle Stress along length

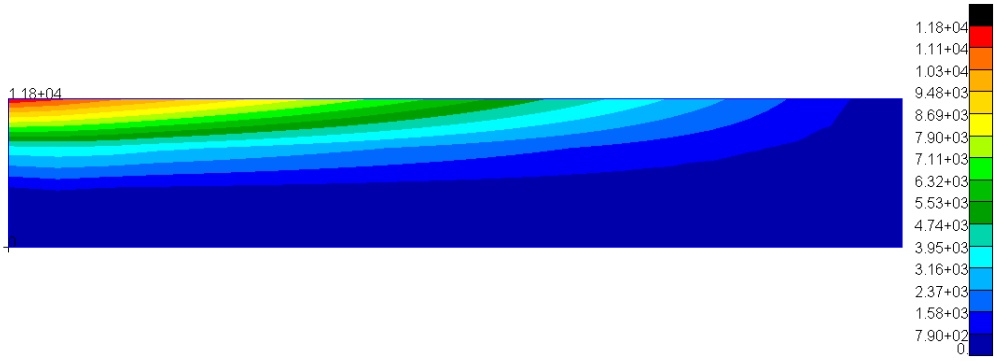

Fig. 6.2.1.2 Rect1 Maximum Principle Stress Fringe Plot

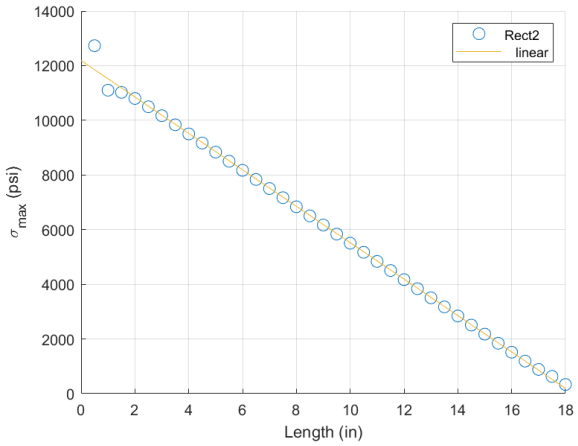

Fig. 6.2.1.3 Model Rect2 Maximum Principle Stress along length

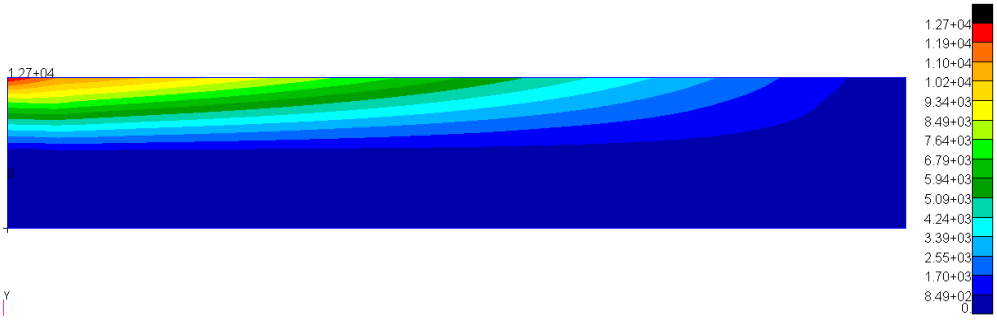

Fig. 6.2.1.4 Rect2 Maximum Principle Stress Fringe Plot

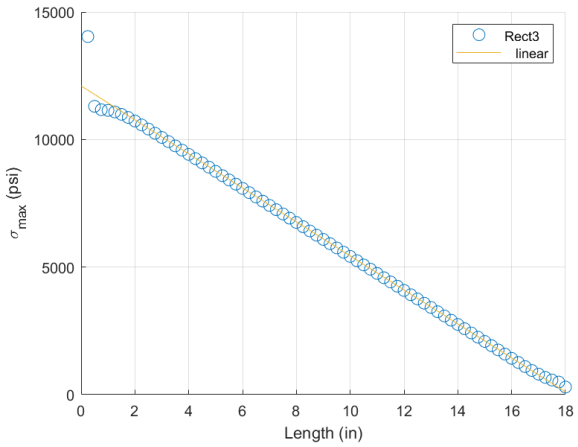

Fig. 6.2.1.5 Model Rect3 Maximum Principle Stress along length

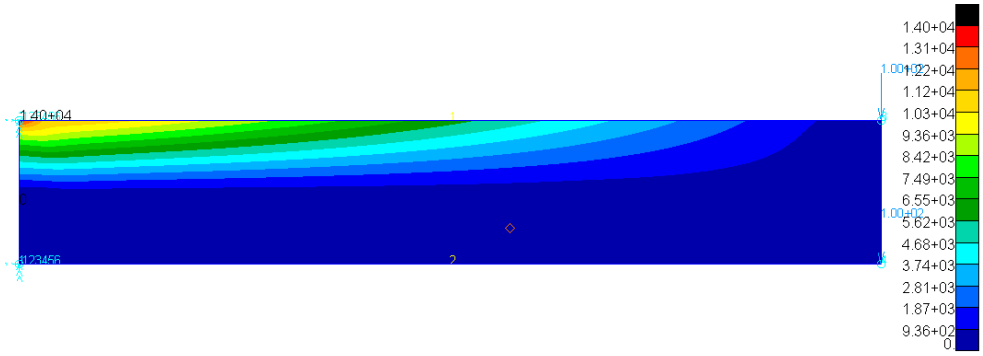

Fig. 6.2.1.6 Rect3 Maximum Principle Stress Fringe Plot

The graphs show a unusual spike in the stress in the final element of each model, Element 1 in all models. This is an imaginary stress caused by unrealistic boundary conditions at the attachment point. A linear line of best fit is added to show a more realistic stress curve for the models.

We see a similar behavior in Models Tri1, Tri2, and Tri3, shown in Figures 6.2.1.7 , 6.2.1.9 , and 6.2.1.11 respectively.

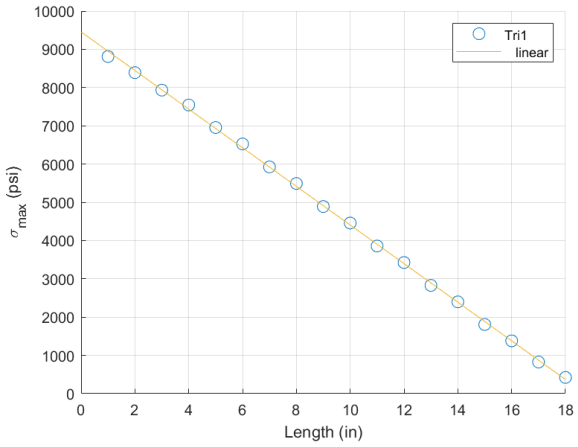

Fig. 6.2.1.7 Model Tri1 Maximum Principle Stress along length

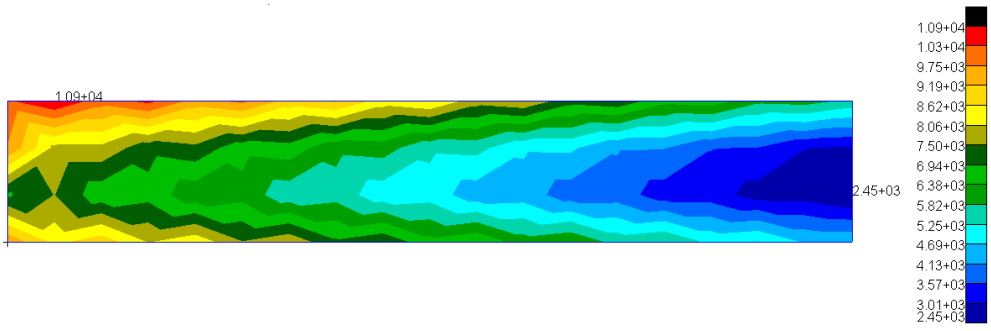

Fig. 6.2.1.8 Tri1 Maximum Principle Stress Fringe Plot

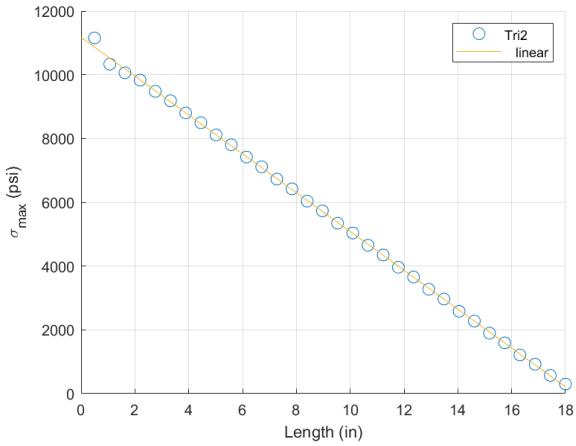

Fig. 6.2.1.9 Model Tri2 Maximum Principle Stress along length

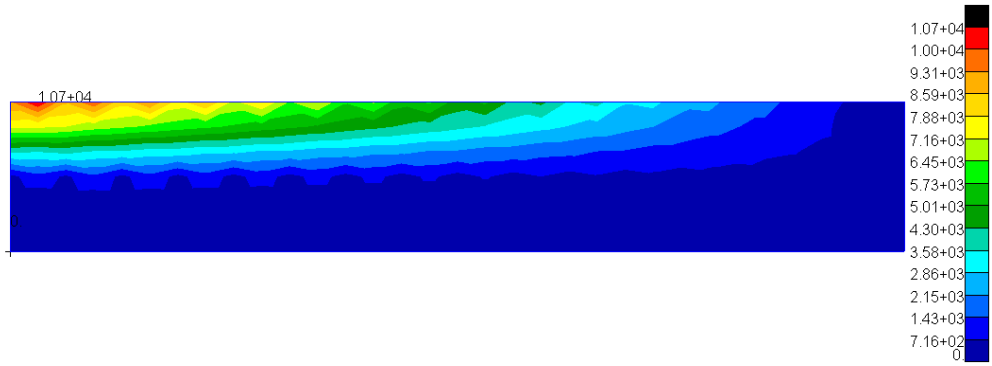

Fig. 6.2.1.10 Tri2 Maximum Principle Stress Fringe Plot

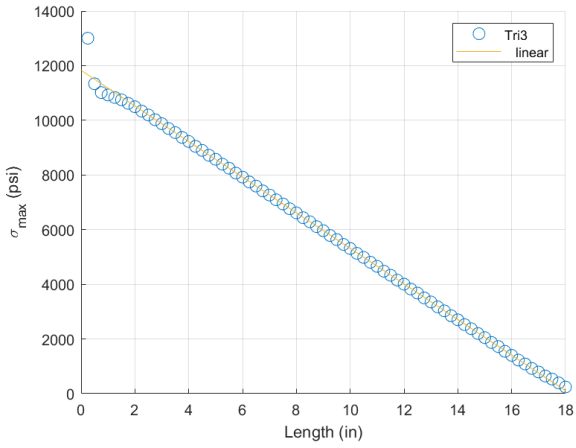

Fig. 6.2.1.11 Model Tri3 Maximum Principle Stress along length

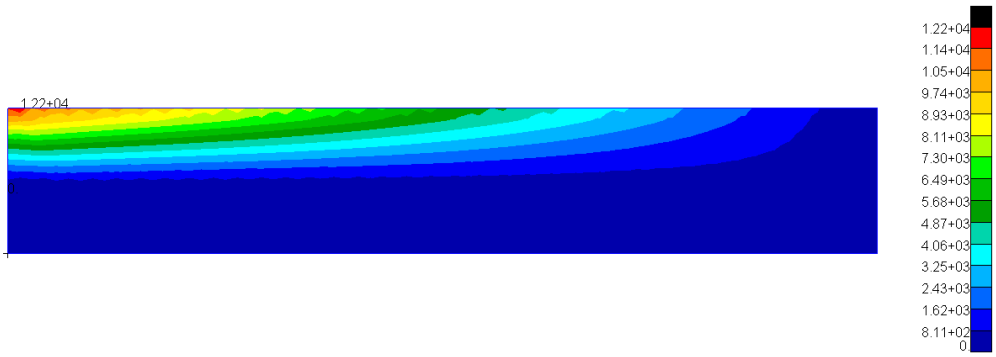

Fig. 6.2.1.12 Tri3 Maximum Principle Stress Fringe Plot

Because of the phenomena caused by the boundary conditions, The 2nd element along the top edge was used as a reference as shown for the maximum principle stress for means of determining convergence. This can be seen in the results, where the maximum principle stress spikes to over 12, 000 psi at Element 1.

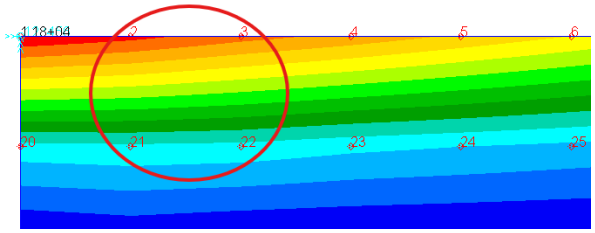

Fig. 6.2.1.13 Element of Interest

6.3 Model Convergence

To determine the accuracy of the models for the amount of elements in the mesh, convergence plots picturing the maximum principle stress versus the degrees of freedom in the model were created for the rectangular and triangular meshing methods, shown in Figures 6.3.0.1 and 6.3.0.2 .

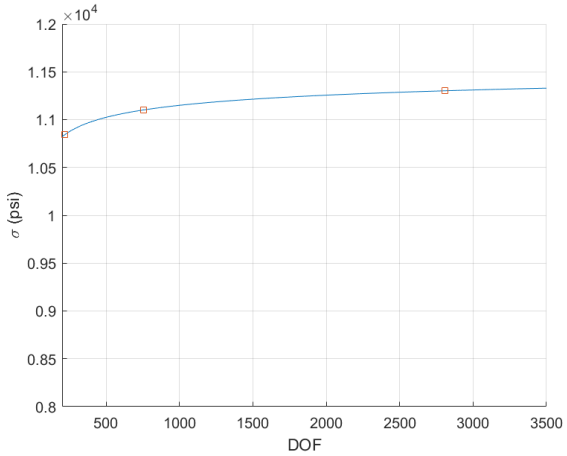

Fig. 6.3.0.1 Rectangular Model Stress Convergence

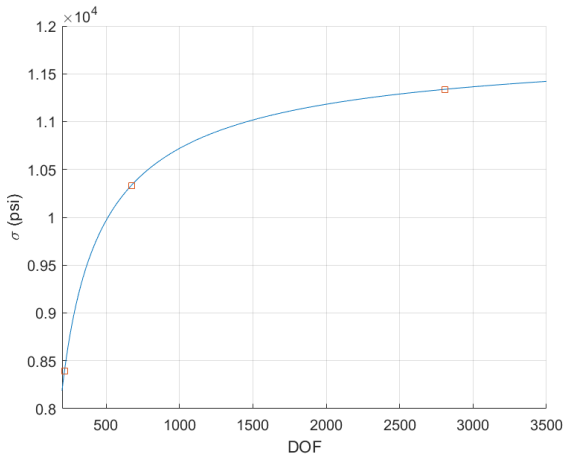

Fig. 6.3.0.2 Triangular Model Stress Convergence

From the figures, the reduced accuracy from the triangular models at lower mesh densities is immediately noticeable but quickly catches up with the rectangular models.

Similar convergence plots were created showing the maximum displacement at the end of the rod versus the degrees of freedom in the model, shown in Figures 6.3.0.3 and 6.3.0.4 .

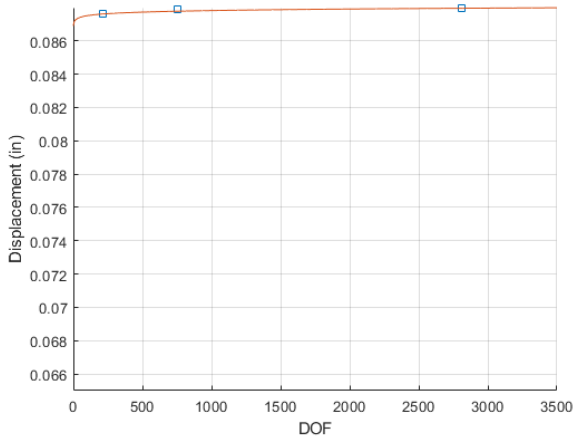

Fig. 6.3.0.3 Rectangular Model Displacement Convergence

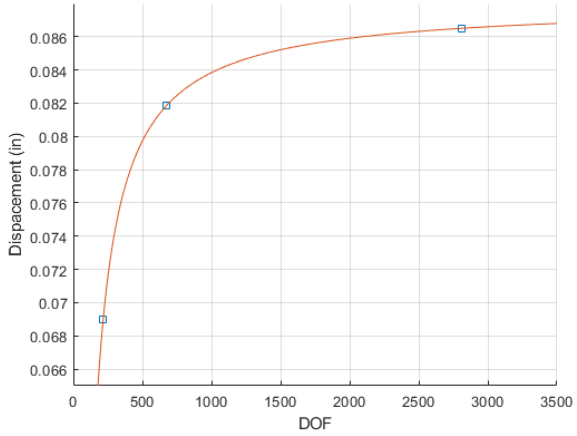

Fig. 6.3.0.4 Triangular Model Displacement Convergence

Both methods show similar convergence results, showing that the models may need to be meshed more finely to properly converge.

Percent Error between mode iterations The percent error between the n-th and $(n+1)$-th iterations is given by the formula:

$$\text{Percent Error} = \left| \frac{x_{n+1} - x_n}{x_n} \right| \times 100$$

where:

- x_n is the result from the n-th iteration,
- x_{n+1} is the result from the $(n+1)$-th iteration.

The two convergence methods were analyzed using the equation above, as shown in table 6.3.1 . The models using rectangular elements is shown have better convergence with the iteration steps with $< 5\%$ error between the final models using both methods, with the triangular models having an error of $> 5\%$ using both methods.

Meshing Type	% Error σ_{max}	% Error Displacement
Rectangular	1.8010	0.1104
Triangular	9.7235	5.6608

Table 6.3.1 Percent Difference Between Final Iterations

Model Stress Comparisons Comparing the stress gradient on the top surface of the models illustrates that as the degrees of freedom increase in the models, the meshing methods converge. Figure 6.3.0.5 shows both models with 126 degrees of freedom. While both models have inaccuracies, the difference in accuracy is wildly different between meshing types even with the same degrees of freedom. Figure 6.3.0.6 shows both models with 2808 degrees of freedom. At this scale, the models have similar stress gradients with only minor discrepancies at the boundary condition.

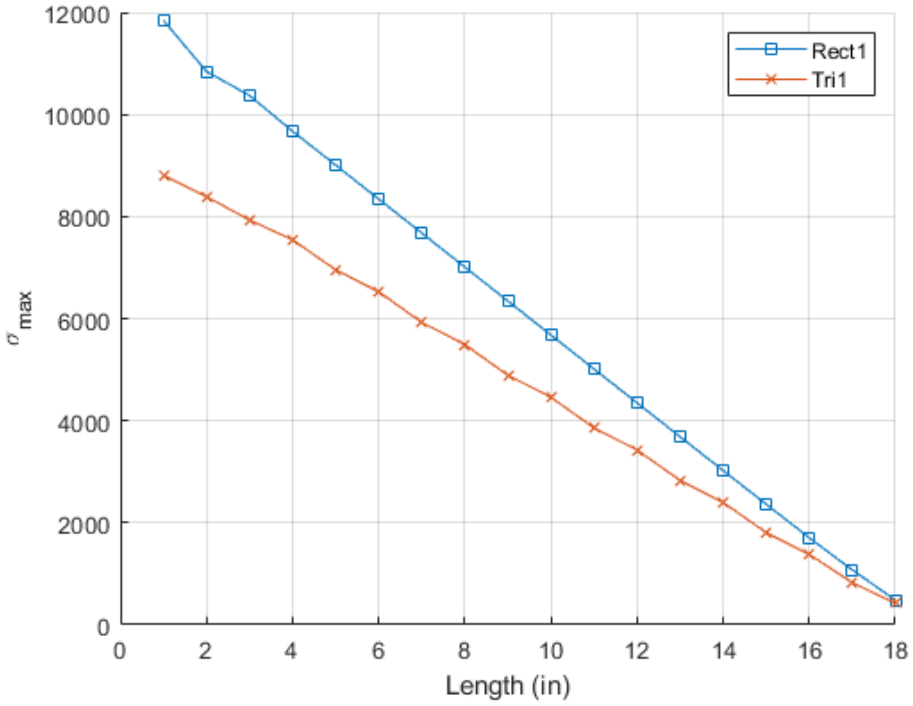

Fig. 6.3.0.5 Rect1 vs. Tri1 (σ_{max})

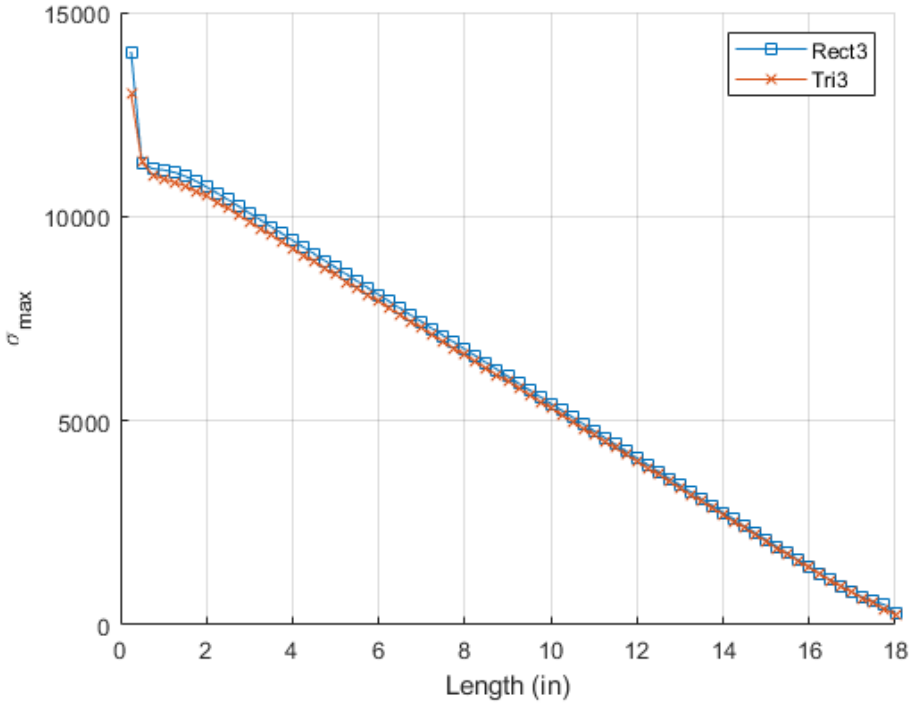

Fig. 6.3.0.6 Rect3 vs. Tri3 (σ_{max})

6.4 Model Comparison with Beam Elements

To validate the membrane element models, a simplified analytical model was created using a classical beam element with identical geometry and boundary conditions. This beam model serves as a benchmark, which assumes linear-elastic behavior, small deformations, and plane sections remaining plane.

The comparison focuses on maximum displacement at the free end of the structure, where deformation is expected to be largest under the applied loading. Figure 6.4.0.1 illustrates the stress and displacement contours of the beam model under the same loading configuration, with a maximum stress of $12,000$ psi (shown in red).

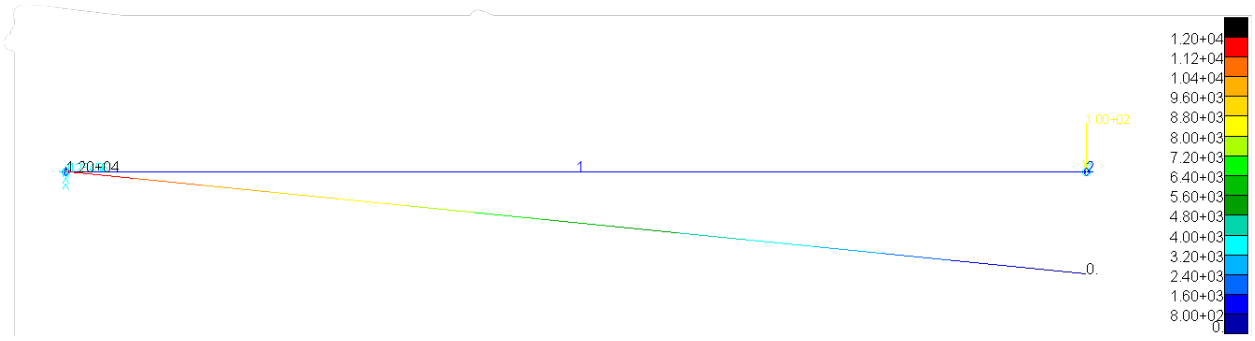

Fig. 6.4.0.1 Beam Model Stress and Displacement Distribution

Table 6.4.1 summarizes the maximum displacement results obtained from the high-resolution membrane models (Rect3 and Tri3) and the beam theory solution. Despite the considerable difference in degrees of freedom (DOFs), all three models predict a very similar displacement magnitude, with differences below 0.2%.

Model	DOFs	Max Displacement (in)
Rect3	2808	-8.798×10^{-2}
Tri3	2808	-8.652×10^{-2}
Beam	6	-8.829×10^{-2}

Table 6.4.1 Comparison of Maximum Displacement with Beam Theory

These results reinforce that both membrane element models, when sufficiently refined, can accurately replicate the structural response predicted by classical beam theory. The beam model's analytical nature makes it a valuable tool for verifying numerical convergence and modeling accuracy. However, unlike the membrane elements, beam theory does not capture the stress distribution along the beam, providing less insight with unusually loaded models.

7. Summary

This analysis investigated the stress and displacement behavior of a cantilevered structure using various finite element mesh strategies, specifically rectangular and triangular membrane elements. The objective was to assess model accuracy, evaluate convergence characteristics, and validate results against a classical beam theory benchmark.

Stress convergence was evaluated by tracking the maximum principal stress at a consistent location across mesh refinements. Rectangular meshes demonstrated faster and more stable convergence compared to triangular meshes, achieving below 2% error in the final iteration. Triangular meshes exhibited larger error margins but showed improvement with increasing refinement.

Displacement convergence was also tracked at the free end of the structure. Both mesh types showed good agreement with beam theory predictions, with displacements converging within 0.2% of the analytical solution.

A beam element model was used as a baseline for comparison. Despite its simplicity and low degrees of freedom, the beam model produced displacement results nearly identical to those from the most refined membrane element models. This validates the overall fidelity of the membrane modeling approach when appropriate meshing is applied.

Ultimately, this study demonstrates that:

- Rectangular membrane meshes are more efficient for capturing stress convergence.
- Triangular elements can yield comparable accuracy, but require finer meshing.
- Finite element models can reliably reproduce analytical solutions when refined appropriately.

The convergence behavior and validation against beam theory affirm the reliability of the chosen modeling strategies, supporting their use in structural simulations where both stress gradients and displacements are of interest.

Appendix

Exerpts from F06 File

S T R E S S E S I N Q U A D R I L A T E R A L E L E M E N T S (Q U A D 4) OPTION = BILIN

	ELEMENT ID	GRID-ID	FIBER DISTANCE	STRESSES IN ELEMENT COORD SYSTEM NORMAL-X	NORMAL-Y	SHEAR-XY	PRINCIPAL STRESSES (ZERO SHEAR) ANGLE	MAJOR	MINOR	VON MISES
0	1	CEN/4	-5.000000E-02	7.792616E+03	1.048207E+03	4.393670E+02	3.7116	7.821118E+03	1.019704E+03	7.364405E+03
			5.000000E-02	7.792616E+03	1.048207E+03	4.393670E+02	3.7116	7.821118E+03	1.019704E+03	7.364405E+03
		1	-5.000000E-02	1.182403E+04	2.493637E+03	4.393670E+02	2.6901	1.184468E+04	2.472993E+03	1.082221E+04
			5.000000E-02	1.182403E+04	2.493637E+03	4.393670E+02	2.6901	1.184468E+04	2.472993E+03	1.082221E+04
		2	-5.000000E-02	1.182403E+04	-3.972240E+02	4.393670E+02	2.0563	1.183981E+04	-4.129993E+02	1.205162E+04
			5.000000E-02	1.182403E+04	-3.972240E+02	4.393670E+02	2.0563	1.183981E+04	-4.129993E+02	1.205162E+04
		21	-5.000000E-02	3.761199E+03	-3.972240E+02	4.393670E+02	5.9659	3.807114E+03	-4.431392E+02	4.046921E+03
			5.000000E-02	3.761199E+03	-3.972240E+02	4.393670E+02	5.9659	3.807114E+03	-4.431392E+02	4.046921E+03
		20	-5.000000E-02	3.761199E+03	2.493637E+03	4.393670E+02	17.3658	3.898600E+03	2.356236E+03	3.400722E+03
			5.000000E-02	3.761199E+03	2.493637E+03	4.393670E+02	17.3658	3.898600E+03	2.356236E+03	3.400722E+03
0	2	CEN/4	-5.000000E-02	7.341394E+03	-2.051100E+02	1.902489E+02	1.4432	7.346187E+03	-2.099032E+02	7.453356E+03
			5.000000E-02	7.341394E+03	-2.051100E+02	1.902489E+02	1.4432	7.346187E+03	-2.099032E+02	7.453356E+03
		2	-5.000000E-02	1.083763E+04	-5.416148E+02	1.902489E+02	0.9576	1.084081E+04	-5.447947E+02	1.112322E+04
			5.000000E-02	1.083763E+04	-5.416148E+02	1.902489E+02	0.9576	1.084081E+04	-5.447947E+02	1.112322E+04
		3	-5.000000E-02	1.083763E+04	1.313948E+02	1.902489E+02	1.0177	1.084101E+04	1.280151E+02	1.077757E+04
			5.000000E-02	1.083763E+04	1.313948E+02	1.902489E+02	1.0177	1.084101E+04	1.280151E+02	1.077757E+04
		22	-5.000000E-02	3.845161E+03	1.313948E+02	1.902489E+02	2.9249	3.854882E+03	1.216742E+02	3.795508E+03
			5.000000E-02	3.845161E+03	1.313948E+02	1.902489E+02	2.9249	3.854882E+03	1.216742E+02	3.795508E+03
		21	-5.000000E-02	3.845161E+03	-5.416148E+02	1.902489E+02	2.4786	3.853397E+03	-5.498502E+02	4.155694E+03
			5.000000E-02	3.845161E+03	-5.416148E+02	1.902489E+02	2.4786	3.853397E+03	-5.498502E+02	4.155694E+03

Fig. 7.0.0.1 Rect1 f06

S T R E S S E S I N Q U A D R I L A T E R A L E L E M E N T S (Q U A D 4) OPTION = BILIN

ELEMENT ID	GRID-ID	FIBER DISTANCE	STRESSES IN ELEMENT COORD SYSTEM NORMAL-X	NORMAL-Y	SHEAR-XY	PRINCIPAL STRESSES (ZERO SHEAR) ANGLE	MAJOR	MINOR	VON MISES
0 1	CEN/4	-5.000000E-02	1.007337E+04	1.523110E+03	8.274215E+02	5.4769	1.015271E+04	1.443776E+03	9.513346E+03
		5.000000E-02	1.007337E+04	1.523110E+03	8.274215E+02	5.4769	1.015271E+04	1.443776E+03	9.513346E+03
	1	-5.000000E-02	1.265855E+04	3.223480E+03	8.274215E+02	4.9740	1.273057E+04	3.151468E+03	1.148386E+04
		5.000000E-02	1.265855E+04	3.223480E+03	8.274215E+02	4.9740	1.273057E+04	3.151468E+03	1.148386E+04
	2	-5.000000E-02	1.265855E+04	-1.772593E+02	8.274215E+02	3.6731	1.271167E+04	-2.303767E+02	1.282841E+04
		5.000000E-02	1.265855E+04	-1.772593E+02	8.274215E+02	3.6731	1.271167E+04	-2.303767E+02	1.282841E+04
	39	-5.000000E-02	7.488195E+03	-1.772593E+02	8.274215E+02	6.0911	7.576491E+03	-2.655555E+02	7.712698E+03
		5.000000E-02	7.488195E+03	-1.772593E+02	8.274215E+02	6.0911	7.576491E+03	-2.655555E+02	7.712698E+03
	38	-5.000000E-02	7.488195E+03	3.223480E+03	8.274215E+02	10.6039	7.643101E+03	3.068574E+03	6.661810E+03
		5.000000E-02	7.488195E+03	3.223480E+03	8.274215E+02	10.6039	7.643101E+03	3.068574E+03	6.661810E+03
0 2	CEN/4	-5.000000E-02	9.494685E+03	-1.281591E+02	7.735382E+01	0.4605	9.495307E+03	-1.287809E+02	9.560348E+03
		5.000000E-02	9.494685E+03	-1.281591E+02	7.735382E+01	0.4605	9.495307E+03	-1.287809E+02	9.560348E+03
	2	-5.000000E-02	1.110161E+04	-3.624400E+02	7.735382E+01	0.3866	1.110213E+04	-3.629619E+02	1.128799E+04
		5.000000E-02	1.110161E+04	-3.624400E+02	7.735382E+01	0.3866	1.110213E+04	-3.629619E+02	1.128799E+04
	3	-5.000000E-02	1.110161E+04	1.061217E+02	7.735382E+01	0.4031	1.110215E+04	1.055776E+02	1.104974E+04
		5.000000E-02	1.110161E+04	1.061217E+02	7.735382E+01	0.4031	1.110215E+04	1.055776E+02	1.104974E+04
	40	-5.000000E-02	7.887762E+03	1.061217E+02	7.735382E+01	0.5695	7.888531E+03	1.053529E+02	7.836386E+03
		5.000000E-02	7.887762E+03	1.061217E+02	7.735382E+01	0.5695	7.888531E+03	1.053529E+02	7.836386E+03
	39	-5.000000E-02	7.887762E+03	-3.624400E+02	7.735382E+01	0.5371	7.888487E+03	-3.631652E+02	8.076196E+03
		5.000000E-02	7.887762E+03	-3.624400E+02	7.735382E+01	0.5371	7.888487E+03	-3.631652E+02	8.076196E+03

Fig. 7.0.0.2 Rect2 f06

S T R E S S E S I N Q U A D R I L A T E R A L E L E M E N T S (Q U A D 4) OPTION = BILIN

ELEMENT ID	GRID-ID	FIBER DISTANCE	STRESSES IN ELEMENT COORD SYSTEM NORMAL-X	NORMAL-Y	SHEAR-XY	PRINCIPAL STRESSES (ZERO SHEAR) ANGLE	MAJOR	MINOR	VON MISES
0 1	CEN/4	-5.000000E-02	1.171603E+04	1.903907E+03	1.350549E+03	7.6956	1.189852E+04	1.721411E+03	1.113804E+04
		5.000000E-02	1.171603E+04	1.903907E+03	1.350549E+03	7.6956	1.189852E+04	1.721411E+03	1.113804E+04
	1	-5.000000E-02	1.386031E+04	3.749128E+03	1.350549E+03	7.4784	1.403760E+04	3.571844E+03	1.263614E+04
		5.000000E-02	1.386031E+04	3.749128E+03	1.350549E+03	7.4784	1.403760E+04	3.571844E+03	1.263614E+04
	2	-5.000000E-02	1.386031E+04	5.868566E+01	1.350549E+03	5.5367	1.399123E+04	-7.222958E+01	1.402748E+04
		5.000000E-02	1.386031E+04	5.868566E+01	1.350549E+03	5.5367	1.399123E+04	-7.222958E+01	1.402748E+04
	75	-5.000000E-02	9.571740E+03	5.868566E+01	1.350549E+03	7.9256	9.759759E+03	-1.293329E+02	9.825064E+03
		5.000000E-02	9.571740E+03	5.868566E+01	1.350549E+03	7.9256	9.759759E+03	-1.293329E+02	9.825064E+03
	74	-5.000000E-02	9.571740E+03	3.749128E+03	1.350549E+03	12.4432	9.869746E+03	3.451122E+03	8.675277E+03
		5.000000E-02	9.571740E+03	3.749128E+03	1.350549E+03	12.4432	9.869746E+03	3.451122E+03	8.675277E+03
0 2	CEN/4	-5.000000E-02	1.071409E+04	-3.299667E+01	1.710249E+02	0.9115	1.071681E+04	-3.571761E+01	1.073471E+04
		5.000000E-02	1.071409E+04	-3.299667E+01	1.710249E+02	0.9115	1.071681E+04	-3.571761E+01	1.073471E+04
	2	-5.000000E-02	1.129947E+04	-2.619347E+02	1.710249E+02	0.8473	1.130200E+04	-2.644640E+02	1.143652E+04
		5.000000E-02	1.129947E+04	-2.619347E+02	1.710249E+02	0.8473	1.130200E+04	-2.644640E+02	1.143652E+04
	3	-5.000000E-02	1.129947E+04	1.959413E+02	1.710249E+02	0.8822	1.130210E+04	1.933077E+02	1.120670E+04
		5.000000E-02	1.129947E+04	1.959413E+02	1.710249E+02	0.8822	1.130210E+04	1.933077E+02	1.120670E+04
	76	-5.000000E-02	1.012871E+04	1.959413E+02	1.710249E+02	0.9861	1.013165E+04	1.929974E+02	1.003654E+04
		5.000000E-02	1.012871E+04	1.959413E+02	1.710249E+02	0.9861	1.013165E+04	1.929974E+02	1.003654E+04
	75	-5.000000E-02	1.012871E+04	-2.619347E+02	1.710249E+02	0.9427	1.013152E+04	-2.647489E+02	1.026646E+04
		5.000000E-02	1.012871E+04	-2.619347E+02	1.710249E+02	0.9427	1.013152E+04	-2.647489E+02	1.026646E+04

Fig. 7.0.0.3 Rect3 f06

S T R E S S E S I N T R I A N G U L A R E L E M E N T S (T R I A 3)

	ELEMENT ID.	FIBER DISTANCE	STRESSES IN ELEMENT COORD SYSTEM NORMAL-X	NORMAL-Y	SHEAR-XY	PRINCIPAL STRESSES (ZERO SHEAR) ANGLE	MAJOR	MINOR	VON MISES
0	1	-5.000000E-02	2.953550E+03	9.451359E+02	9.207649E+02	21.2590	3.311782E+03	5.869040E+02	3.060826E+03
		5.000000E-02	2.953550E+03	9.451359E+02	9.207649E+02	21.2590	3.311782E+03	5.869040E+02	3.060826E+03
0	2	-5.000000E-02	8.803400E+03	-3.994617E+02	-2.396789E+02	-1.4909	8.809638E+03	-4.056997E+02	9.019333E+03
		5.000000E-02	8.803400E+03	-3.994617E+02	-2.396789E+02	-1.4909	8.809638E+03	-4.056997E+02	9.019333E+03
0	3	-5.000000E-02	8.333450E+03	-5.498456E+02	7.096284E+02	4.5386	8.389781E+03	-6.061760E+02	8.708705E+03
		5.000000E-02	8.333450E+03	-5.498456E+02	7.096284E+02	4.5386	8.389781E+03	-6.061760E+02	8.708705E+03
0	4	-5.000000E-02	3.168701E+03	5.388993E+02	-3.402514E+02	-7.2540	3.212011E+03	4.955899E+02	2.995127E+03
		5.000000E-02	3.168701E+03	5.388993E+02	-3.402514E+02	-7.2540	3.212011E+03	4.955899E+02	2.995127E+03

Fig. 7.0.0.4 Tri1 f06

S T R E S S E S I N T R I A N G U L A R E L E M E N T S (T R I A 3)

	ELEMENT ID.	FIBER DISTANCE	STRESSES IN ELEMENT COORD SYSTEM NORMAL-X	NORMAL-Y	SHEAR-XY	PRINCIPAL STRESSES (ZERO SHEAR) ANGLE	MAJOR	MINOR	VON MISES
0	1	-5.000000E-02	7.195671E+03	2.302615E+03	1.041490E+03	11.5298	7.408128E+03	2.090158E+03	6.615509E+03
		5.000000E-02	7.195671E+03	2.302615E+03	1.041490E+03	11.5298	7.408128E+03	2.090158E+03	6.615509E+03
0	2	-5.000000E-02	1.114845E+04	1.681305E+01	2.408857E+02	1.2391	1.115366E+04	1.160279E+01	1.114786E+04
		5.000000E-02	1.114845E+04	1.681305E+01	2.408857E+02	1.2391	1.115366E+04	1.160279E+01	1.114786E+04
0	3	-5.000000E-02	1.030906E+04	-2.517905E+02	5.052354E+02	2.7327	1.033318E+04	-2.759061E+02	1.047386E+04
		5.000000E-02	1.030906E+04	-2.517905E+02	5.052354E+02	2.7327	1.033318E+04	-2.759061E+02	1.047386E+04
0	4	-5.000000E-02	7.423789E+03	4.236848E+02	-2.780912E+02	-2.2714	7.434819E+03	4.126545E+02	7.237321E+03
		5.000000E-02	7.423789E+03	4.236848E+02	-2.780912E+02	-2.2714	7.434819E+03	4.126545E+02	7.237321E+03

Fig. 7.0.0.5 Tri2 f06

S T R E S S E S I N T R I A N G U L A R E L E M E N T S (T R I A 3)

	ELEMENT ID.	FIBER DISTANCE	STRESSES IN ELEMENT COORD SYSTEM NORMAL-X	NORMAL-Y	SHEAR-XY	PRINCIPAL STRESSES (ZERO SHEAR) ANGLE	MAJOR	MINOR	VON MISES
0	1	-5.000000E-02	9.727839E+03	3.112909E+03	1.329357E+03	10.9482	9.984994E+03	2.855754E+03	8.907343E+03
		5.000000E-02	9.727839E+03	3.112909E+03	1.329357E+03	10.9482	9.984994E+03	2.855754E+03	8.907343E+03
0	2	-5.000000E-02	1.289689E+04	6.198602E+02	1.155235E+03	5.3290	1.300465E+04	5.121015E+02	1.275631E+04
		5.000000E-02	1.289689E+04	6.198602E+02	1.155235E+03	5.3290	1.300465E+04	5.121015E+02	1.275631E+04
0	3	-5.000000E-02	1.132226E+04	1.159776E+02	4.193976E+02	2.1403	1.133793E+04	1.003035E+02	1.128811E+04
		5.000000E-02	1.132226E+04	1.159776E+02	4.193976E+02	2.1403	1.133793E+04	1.003035E+02	1.128811E+04
0	4	-5.000000E-02	9.975059E+03	3.187465E+02	1.246201E+02	0.7393	9.976667E+03	3.171385E+02	9.821938E+03
		5.000000E-02	9.975059E+03	3.187465E+02	1.246201E+02	0.7393	9.976667E+03	3.171385E+02	9.821938E+03

Fig. 7.0.0.6 Tri3 f06

S T R E S S E S I N B A R E L E M E N T S (C B A R)

	ELEMENT ID.	SA1 SB1	SA2 SB2	SA3 SB3	SA4 SB4	AXIAL STRESS	SA-MAX SB-MAX	SA-MIN SB-MIN	M.S.-T M.S.-C
0	1	1.200000E+04	-1.200000E+04	-1.200000E+04	1.200000E+04	0.0	1.200000E+04	-1.200000E+04	
		-4.547473E-12	4.547473E-12	4.547473E-12	-4.547473E-12		4.547473E-12	-4.547473E-12	

Fig. 7.0.0.7 Beam Stress f06

0 MAXIMUM DISPLACEMENTS

	SUBCASE/ DAREA ID	T1	T2	T3	R1	R2	R3
0	1	0.0000000E+00	8.8294733E-02	0.0000000E+00	0.0000000E+00	0.0000000E+00	7.1999997E-03

1 MSC.NASTRAN JOB CREATED ON 23-APR-25 AT 21:45:28 APRIL 23, 2025 MSC Nastran 5/13/24 PAGE 10

Fig. 7.0.0.8 Beam Displacement f06

References

[1] "MSC Patran," , 2024.